10

Heat Conduction for Helical and Periodical Contact in a Mine Hoist

Yu-xing Peng, Zhen-cai Zhu and Guo-an Chen
School of Mechanical and Electrical Engineering, China University of Mining and Technology, Xuzhou, China

1. Introduction

Mine hoist is the "throat" of mine production, which plays the role of conveying coal, underground equipments and miners. Fig. 1 shows the schematic of mining friction hoist. The friction lining is fixed outside the drum and the wire rope is hung on the drum. It is dependent on friction force between friction lining and wire rope to lift miner, coal and equipment during the process of mine hoisting. Accordingly, the reliability of mine hoist is up to the friction force between friction lining and wire rope. Therefore, the friction lining is one of the most important parts in mine hoisting system. In addition, the disc brake for mine hoist is shown in Fig. 1 and it is composed of brake disc and brake shoes. During the braking process, the brake shoes are pushed onto the disc with a certain pressure, and the friction force generated between them is applied to brake the drum of mine hoist. And the disc brake is the most significant device for insuring the safety of mine hoist. Therefore, several strict rules for disc brake and friction lining are listed in "Safety Regulations for Coal Mine" in China (Editorial Committee of Mine Safety Handbooks, 2004).

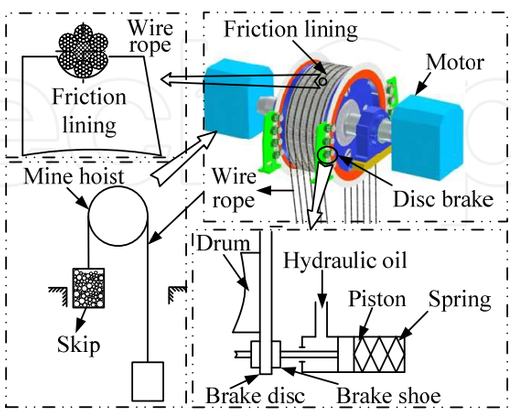

Fig. 1. Schematic of mine friction hoist

Under the condition of overload, overwinding or overfalling of a mine hoist, the high-speed slide occurs between friction lining and wire rope which will results in a serious accident. At

this situation, the disc brake would be acted to brake the drum with large pressure, which is called a emergency brake. And a large amount of friction heat accumulates on the friction surface of friction lining and disc brake during the braking process. This leads to the decrease of mechanical property on the contact surface, which reduces the tribological properties and makes the hoist accident more serious. Therefore, it is necessary to study the heat conduction of friction lining and disc brake during the high-speed slide accident in a mine hoist.

The heat conduction of friction lining has been studied (Peng et al., 2008; Liu & Mei, 1997; Xia & Ge, 1990; Yang, 1990). However, the previous work neglected the non-complete helical contact between friction lining and wire rope. Besides, the previous results were based on the static thermophysical property (STP). But the friction lining is a kind of polymer and the thermophysical properties (specific heat capacity, thermal diffusivity and thermal conductivity) vary with the temperature (Singh et al., 2008; Isoda & Kawashima, 2007; He et al., 2005; Hegeman et al., 2005; Mazzone, 2005). Therefore, the temperature field calculated by STP is inconsistent with the actual temperature field. The methods solving the heat-conduction equation include the method of separation of variables (Golebiowski & Kwieckowski, 2002; Lukyanov, 2001), Laplace transformation method (Matysiak et al., 2002; Yevtushenko & Ivanyk, 1997), Green's function method (Naji & Al-Nimr, 2001), integral-transform method (Zhu et al., 2009), finite element method (Voldrich, 2007; Qi & Day, 2007; Thuresson, 2006; Choi & Lee, 2004) and finite difference method [Chang & Li, 2008; Liu et al., 2009], etc. The former three methods are analytic solution methods and it is difficult to solve the heat-conduction problem with the dynamic theromophysical property (DTP) and complicate boundary conditions. Though the integral-transform method is a numerical solution method and is suitable for solving the problem of non-homogeneous transient heat conduction, it is incapable of solving the nonlinear problem. Additionally, both the finite element method and finite difference method could solve nonlinear heat-conduction problem. However, the finite difference expression of the partial differential equation is simpler than finite element expression. Thereby, the finite difference method is adopted to solve the nonlinear heat-conduction problem with DTP and non-complete helical contact characteristics.

It is depend on the friction force between brake shoe and brake disc to brake the drum of mine hoist. So the safety and reliability of disc brake are mainly determined by the tribological properties of its friction pair. The tribological properties of brake shoe were studied (Zhu et al., 2008, 2006), and it was found that the temperature rise of disc brake affects its tribological properties seriously during the braking process, which in turn threatens the braking safety directly. Presently, most investigations on the temperature field of disc brake focused only on the operating conditions of automobile. The temperature field of brake disc and brake shoe was analyzed in an automobile under the emergency braking condition (Cao & Lin, 2002; Wang, 2001). The effects of parameters of operating condition on the temperature field of brake disc (Lin et al., 2006). Ma adopted the concept of whole and partial heat-flux, and considered that the temperature rise of contact surface was composed of partial and nominal temperature rise (Ma et al., 1999). And the theoretical model of heat-flux under the emergency braking condition was established by analyzing the motion of automobile (Ma & Zhu, 1998). However, the braking condition in mine hoist is worse than that in automobile, and the temperature field of its disc brake may show different behaviors. Nevertheless, there are a few studies on the temperature field of mine hoist's disc brake. Zhu investigated the temperature field of brake shoe during emergency braking in mine hoist (Zhu et al., 2009). Bao brought forward a new method of calculating the maximal

surface temperature of brake shoe during mine hoist's emergency braking (Bao et al., 2009). And yet, the above studies were based on the invariable thermophysical properties of brake shoe, and the temperature field of brake disc hasn't been investigated.

In order to master the heat conduction of friction lining and improve the mine safety, the non-complete helical contact characteristics between friction lining and wire rope was analyzed, and the mechanism of dynamic distribution for heat-flow between friction lining and wire rope was studied. Then, the average and partial heat-flow density were analyzed. Consequently, the friction lining's helical temperature field was obtained by applying the finite difference method and the experiment was performed on the friction tester to validate the theoretical results. Furthermore, the heat conduction of disc brake was studied. The temperature field of brake shoe was analyzed with the consideration of its dynamic thermophysical properties. And the brake disc's temperature rise under the periodical heat-flux was also investigated. The research results will supply the theoretical basis with the anti-slip design of mine friction hoist, and our study also has general application to other helical and periodical contact operations.

2. Heat conduction for helical contact

2.1 Helical contact characteristics

In order to obtain the temperature rise of friction lining during sliding contact with wire rope, it is necessary to analyze the contact characteristic between friction lining and wire rope. The schematic of helical contact is shown in Fig. 2.

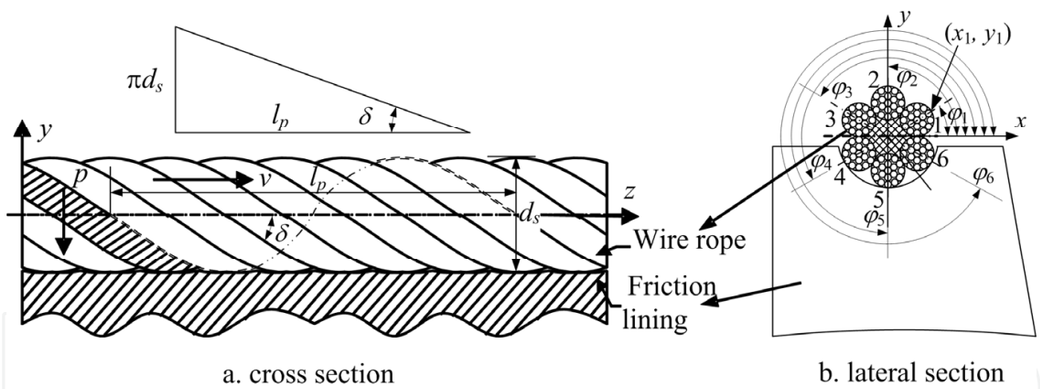

Fig. 2. Schematic of helical contact

For obtaining the exact heat-flow generated by the helical contact, the contact characteristics must be determined firstly. As is shown Fig. 2, the friction lining contacts with the outer strand of wire rope which is a helical structure and the helical equation is as follows

$$\begin{cases} x_i = \dfrac{d_s}{2} \cdot \cos\varphi_i = \dfrac{d_s}{2} \cdot \cos\left[\omega t + \dfrac{\pi}{3} i - \dfrac{\pi}{6}\right] \\ y_i = \dfrac{d_s}{2} \cdot \sin\varphi_i = \dfrac{d_s}{2} \cdot \sin\left[\omega t + \dfrac{\pi}{3} i - \dfrac{\pi}{6}\right] \\ z_i = v \cdot t \end{cases} \tag{1}$$

where j is the helix angle, i is the strand number in the wire rope (i=1, 2, 3,⋯,6), d_s is the diameter of the wire rope, and v is the relative speed between friction lining and wire rope. It is seen from Fig. 2(a) that, any point on the contact surface of friction lining contacts periodically with the outer surface of wire rope because of wire rope's helical structure, and the period for unit pitch is expressed as

$$T_P = \frac{l_p}{v} = \frac{\pi d_s}{\tan\delta \cdot v} \tag{2}$$

where l_p is the pitch of outer strand, d_s is the lay angle of strand ($\delta_s = 0.28$), and $\omega = 2\pi/T_P$ in Eq. (1).

The contact characteristics can be gained according to Eqs. (1) and (2). The variation of j_i corresponding to coordinates x_i and y_i is shown in Fig. 3.

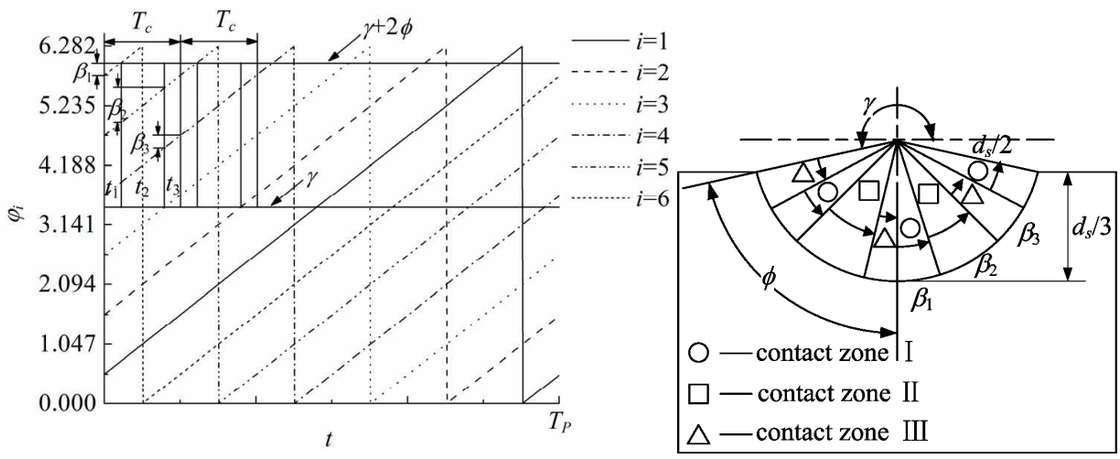

(a) helical angle within the pitch period (b) contact zone

Fig. 3. Schematic of helical contact

From Figs. 3(a) and 3(b), it is observed that the contact period is T_c within the angle (g~g+2f) of the rope groove in the lining, and the contact zone is divided into three regions which is shown in Eq. (3).

$$\begin{aligned}
&\gamma_1 \in \left\{\left(\frac{7}{6}\pi,\ \frac{7}{6}\pi+\beta_1\right),\left(\frac{3}{2}\pi,\ \frac{3}{2}\pi+\beta_1\right),\left(\frac{11}{6}\pi,\ \frac{11}{6}\pi+\beta_1\right)\right\},\\
&\qquad t \in \left(mT_{\mathrm{C}},\ mT_{\mathrm{C}}+t_1\right);\\
&\gamma_2 \in \left\{\left(\frac{7}{6}\pi+\beta_1,\ \frac{7}{6}\pi+\beta_1+\beta_2\right),\left(\frac{3}{2}\pi+\beta_1,\ \frac{3}{2}\pi+\beta_1+\beta_2\right)\right\},\\
&\qquad t \in \left(mT_{\mathrm{C}}+t_1,\ mT_{\mathrm{C}}+t_1+t_2\right);\\
&\gamma_3 \in \left\{\left(\gamma,\ \frac{7}{6}\pi\right),\left(\frac{7}{6}\pi+\beta_1+\beta_2,\ \frac{3}{2}\pi\right),\left(\frac{3}{2}\pi+\beta_1+\beta_2,\ \frac{11}{6}\pi\right)\right\},\\
&\qquad t \in \left(mT_{\mathrm{C}}+t_1+t_2,\ mT_{\mathrm{C}}+T_{\mathrm{C}}\right),\ (m=0,1,2,\cdots);
\end{aligned} \tag{3}$$

where b_s is the angle increment within t_s, t_s is the contact time, $t_s = b_s/w$ (s=1, 2, 3), $T_c = t_1+t_2+t_3$; where $\phi = 1.27$, $\beta_1 = \beta_3 = 0.22, \beta_2 = 0.6$. It is seen from Fig. 3(a) and Fig. 3(b), the lining groove contacts with the outside of wire rope and the number of contact point is two or three. And the contact arc length is unequal. At the certain speed, the contact arc length within t_2 is the longest and the contact arc length within t_2 and t_3 is equal.

2.2 Mechanism of dynamic distribution for heat-flow

2.2.1 Dynamic thermophysical properties of friction lining

At present, the linings G and K are widely used in most of mine friction hoists in China. The lining is kind of polymer whose thermophysical properties are temperature-dependent. In orer to master the friction heat, it is necessary to study their dynamic thermophysical properties. In this study, the selected sample G and K were analyzed, and its thermophysical properties were measured synchronistically on a light-flash heat conductivity apparatus (LFA 447). Given the friction lining's density r, the thermal conductivity is defined by

$$\lambda(T) = \rho \times C_p(T) \times \alpha(T) \tag{4}$$

where C_p is the specific heat capacity and a is the thermal diffusivity

It is seen from Fig. 4(a) that the C_p increases with the temperature and the lining G has higher value of C_p than lining K. In Fig. 4(b), the a decreases with the temperature nonlinearly whose value of lining G is obviously higher than that of K. As shown in Fig. 4(c), the l increases with the temperature below 90°C and keeps approximately stable above 90°C. And the l of lining G is about 0.45lw·m^{-1}k^{-1} within the temperature range (90°C~240°C), while that of lining K is only 0.3w·m^{-1}k^{-1}.

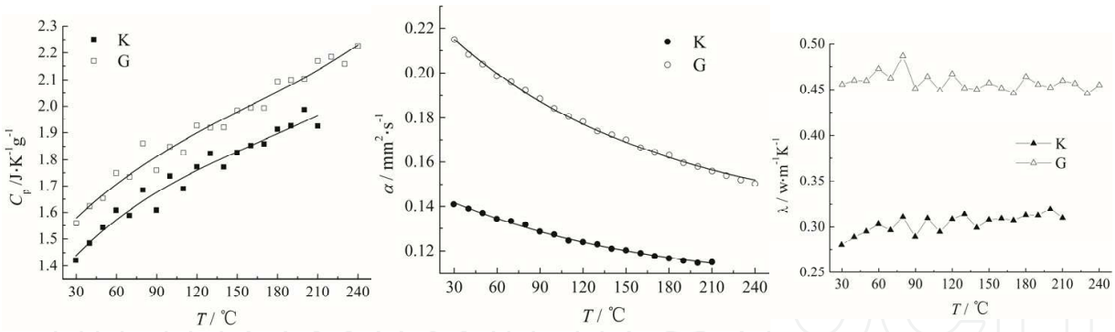

(a) Specific heat capacity (b) Thermal diffusivity (c) Thermal conductivity

Fig. 4. Dynamic thermophysical parameters of friction linings

According to the change rules of specific heat capacity and thermal diffusivity in Fig. 4, the polynomial fit and exponential fit are used to fit curves, and the fitting equations are as follows:

for lining G,

$$\begin{cases} C_p(T) = 1.344 + 8.48 \times 10^{-3} T - 4 \times 10^{-5} T^2 + 1.026 \times 10^{-7} T^3, \ r_0^2 = 0.972 \\ \alpha(T) = 0.132 + 0.0832 \times e^{-\frac{T-30.1}{148.749}}, r_0^2 = 0.998 \end{cases} \tag{5}$$

for lining K,

$$\begin{cases} C_{\mathrm{p}}(T) = 1.272 + 6.31\times10^{-3}T - 2\times10^{-5}T^2 + 4.861\times10^{-8}T^3, \ r_0{}^2 = 0.961 \\ \alpha(T) = 0.104 + 0.0379\times \mathrm{e}^{-\frac{T-29.6}{141.032}}, \ r_0{}^2 = 0.996 \end{cases} \tag{6}$$

where $r_0{}^2$ is the correlation coefficient whose value is close to 1, which indicates that the fitting curves agree well with the experiment results. Consequently, the fitting equation of thermal conductivity of Lining G is deduced by Eqs. (4) and (5).

2.1.2 Dynamic distribution coefficient of heat-flow

In order to master the real temperature field of the friction lining, the distribution coefficient of heat-flow must be determined with accuracy. Suppose the frictional heat is totally transferred to the friction lining and wire rope. According to the literature (Zhu et al., 2009), the dynamic distribution coefficient of heat-flow for the friction lining is obtained

$$k = \frac{q_{\mathrm{f}}}{q_{\mathrm{f}} + q_{\mathrm{W}}} = 1 - \frac{q_{\mathrm{W}}}{q_{\mathrm{f}} + q_{\mathrm{W}}} = 1 - \frac{1}{\frac{q_{\mathrm{f}}}{q_{\mathrm{W}}} + 1} = 1 - \frac{1}{\sqrt{\frac{\rho\, C_{\mathrm{p}} \lambda}{\rho_{\mathrm{w}} C_{\mathrm{pw}} \lambda_{\mathrm{w}}}} + 1} \tag{7}$$

where q_{f} and q_{w} are the heat-flow entering the friction lining and wire rope. r_{w}, C_{pw}, l_{w} and a_{w} are the density, special heat, thermal diffusivity and thermal conductivity of wire rope, respectively.

2.3 Heat-flow density

Determining the friction heat-flow accurately during the sliding process is the important precondition of calculating the temperature field of friction lining. In this study, according to the force analysis of friction lining under the experimental condition, the total heat-flow is studied. And the partial heat-flow on the groove surface of friction lining is gained with the consideration of mechanism of dynamic distribution for heat-flow and helical contact characteristic.

The sliding friction experiment is performed on the friction tester. As shown in Fig. 2, the average heat-flow entering the friction lining under the experiment condition is given as

$$q_{\mathrm{f}} = k \cdot q_{\mathrm{a}} = k \cdot f_1 \cdot p \cdot v \tag{8}$$

where f_1 is the coefficient of friction between friction lining and wire rope, p is the average pressure on the rope groove of friction lining, v is the sliding speed.

According to the helical contact characteristic, the contact period is divided into three time period. Therefore, the partial heat-flow at every time period is obtained on the basis of the contact time

$$q_{\mathrm{f1}} = q_{\mathrm{f}} \frac{t_1}{t_1 + t_2 + t_3}, \ q_{\mathrm{f2}} = q_{\mathrm{f}} \frac{t_2}{t_1 + t_2 + t_3}, \ q_{\mathrm{f3}} = q_{\mathrm{f}} \frac{t_3}{t_1 + t_2 + t_3} \tag{9}$$

2.4 Theoretical analysis on temperature field of friction lining

2.4.1 Theoretical model

On the basis of the above analysis of contact characteristics, it reveals that the temperature field is nonuniform due to the non-complete helical contact between friction lining and wire rope. Moreover, the heat conduction equation is nonlinear on account of DTP. Based on the heat transfer theory, the heat conduction equation, the boundary condition and the initial condition are obtained from Fig. 2:

$$\frac{\partial}{\partial r}\left(\lambda(T)\frac{\partial T}{\partial r}\right)+\frac{\lambda(T)}{r}\frac{\partial T}{\partial r}+\frac{1}{r^2}\frac{\partial}{\partial \theta}\left(\lambda(T)\frac{\partial T}{\partial \theta}\right)=\rho(T)C_{\mathrm{p}}(T)\frac{\partial T}{\partial t} \tag{10}$$

$$\begin{aligned}
&-\lambda\frac{1}{r}\frac{\partial T}{\partial \theta}+h_1T=h_1T_0 \quad (\theta=-\phi,t\geq 0,r_1\leq r\leq r_2) && \text{(a)}\\
&\lambda\frac{1}{r}\frac{\partial T}{\partial \theta}+h_2T=h_2T_0 \quad (\theta=\phi,t\geq 0,r_1\leq r\leq r_2) && \text{(b)}\\
&-\lambda\frac{\partial T}{\partial r}+h_3T=q_{\mathrm{f}}+h_3T_0 \quad (r=r_1,t\geq 0,-\phi\leq\theta\leq\phi) && \text{(c)}\\
&\lambda\frac{\partial T}{\partial r}+h_4T=h_4T_0 \quad (r=r_2,t\geq 0,-\phi\leq\theta\leq\phi) && \text{(d)}\\
&T(r,\theta,\alpha,t)=T_0 \quad (t=0,r_1\leq r\leq r_2,-\phi\leq\theta\leq\phi) && \text{(e)}
\end{aligned} \tag{11}$$

where h_m is the coefficient of convective heat transfer (m=1, 2, 3 , 4).

2.4.2 Solution

The finite difference method is adopted to solve Eqs. (10) and (11), because it is suitable to solve the problem of nonlinear transient heat conduction. Firstly, the solving region is divided into grid with mesh scale of Dr and Dq, and the time step is Dt. And then the friction lining's temperature can be expressed as

$$T(r,\theta,t)=T(r_1+i\Delta r,j\Delta\theta,n\Delta t)=T_{i,j}^{n} \tag{12}$$

The central difference is utilized to express the partial derivatives $\partial T/\partial r$ 、 $\partial(\lambda\partial T/\partial r)/\partial r$ and $\partial(\lambda\partial T/\partial\theta)/\partial\theta$, and their finite difference expressions are obtained

$$\begin{aligned}
&\frac{\partial T}{\partial r}=\frac{T_{i+1,j}-T_{i-1,j}}{2\Delta r}+O(\Delta r)^2 && \text{(a)}\\
&\frac{\partial}{\partial r}\left(\lambda\frac{\partial T}{\partial r}\right)=\frac{\lambda_{i-1/2,j}\left(T^{n+1}{}_{i-1,j}-T^{n+1}{}_{i,j}\right)-\lambda_{i+1/2,j}\left(T^{n+1}{}_{i,j}-T^{n+1}{}_{i+1,j}\right)}{(\Delta r)^2}+O(\Delta r)^2 && \text{(b)}\\
&\frac{\partial}{\partial \theta}\left(\lambda\frac{\partial T}{\partial \theta}\right)=\frac{\lambda_{i-1/2,j}\left(T^{n+1}{}_{i,j-1}-T^{n+1}{}_{i,j}\right)-\lambda_{i+1/2,j}\left(T^{n+1}{}_{i,j}-T^{n+1}{}_{i,j+1}\right)}{(\Delta\theta)^2}+O(\Delta\theta)^2 && \text{(c)}
\end{aligned} \tag{13}$$

Submit Eq. (13) into Eq. (10), the following equation is obtained

$$\frac{\lambda_{i-1/2,j}\left(T^{n+1}{}_{i-1,j}-T^{n+1}{}_{i,j}\right)-\lambda_{i+1/2,j}\left(T^{n+1}{}_{i,j}-T^{n+1}{}_{i+1,j}\right)}{\left(\Delta r\right)^2}+\lambda_{i,j}\frac{T^{n+1}_{i+1,j}-T^{n+1}_{i-1,j}}{2i\Delta r^2}$$
$$+\frac{\lambda_{i-1/2,j}\left(T^{n+1}{}_{i,j-1}-T^{n+1}{}_{i,j}\right)-\lambda_{i+1/2,j}\left(T^{n+1}{}_{i,j}-T^{n+1}{}_{i,j+1}\right)}{i^2\left(\Delta r\Delta\theta\right)^2}=\left(\rho C_{\mathrm{p}}\right)_{i,j}\frac{T^{n+1}_{i,j}-T^{n}_{i,j}}{\Delta t} \tag{14}$$

where the subscript (i-1/2) of l denotes the average thermal conductivity between note i and note i-1, and the subscript (i+1/2) is the average thermal conductivity between note i and note i+1. In the same way, the difference expressions of boundary condition can be gained by the forward difference and backward difference:

$$-\lambda_{i,-N}\frac{T^{n+1}_{i,-N+1}-T^{n+1}_{i,-N}}{i\Delta r\Delta\theta}+h_1T^{n+1}_{i,-N}=h_1T_0\quad(j=-N)\quad(\mathrm{a})$$
$$\lambda_{i,N}\frac{T^{n+1}_{i,N}-T^{n+1}_{i,N-1}}{i\Delta r\Delta\theta}+h_2T^{n+1}_{i,N}=h_2T_0\quad(j=N)\qquad(\mathrm{b})$$
$$-\lambda_{0,j}\frac{T^{n+1}_{1,j}-T^{n+1}_{0,j}}{i\Delta r}+h_3T^{n+1}_{0,j}=q_{\mathrm{f}}+h_3T_0\quad(i=0)\quad(\mathrm{c}) \tag{15}$$
$$-\lambda_{M,j}\frac{T^{n+1}_{M,j}-T^{n+1}_{M-1,j}}{i\Delta r}+h_4T^{n+1}_{M,j}=h_4T_0\quad(i=M)\quad(\mathrm{d})$$
$$T^{0}_{i,j}=T_0\qquad(n=0)\qquad(\mathrm{e})$$

Combined with Eqs. (14) and (15), the friction lining's temperature field is obtained by the iterative computations.

2.5 Experimental study

At present, the non-contact thermal infrared imager is widely used to measure the exposed surface, while the friction surface contacts with each other and it is impossible to gain the

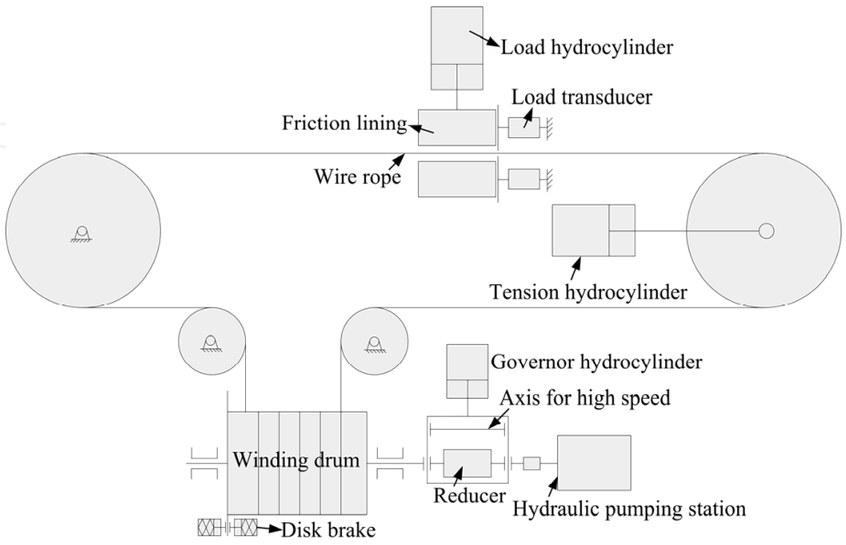

Fig. 5. Schematic of friction tester

surface temperature by the non-contact measurement. Presently, there is no better way to measure the temperature of friction contact surface. In this study, the thermocouple is used to measure to the surface layer temperature, which is embedded in the friction lining and closed to the friction surface. The experiment is performed on the friction tester to study the temperature of friction lining during the friction sliding process. In Fig. 5, the hydraulic pumping station drives the winding drum through the coupling device (axis for high speed or reducer for low speed), and the governor hydrocylinder controls which of the coupling devices would be connected. The wire rope is wrapped on the winding drum, and the motion of the drum leads to the cyclical motion of wire rope. Before the wire rope moves, the tension hydrocylinder makes the wire rope tense and the friction lining is pushed by the load hydrocylinder to clamp the wire rope. Consequently, as the wire rope moves, the friction force is measured by the load transducer and the normal force acted on the wire rope is deduced from the hydraulic pressure of the load hydrocyclinder.

2.5.1 Thermocouple layout

According to the helical contact characteristics, eight thermocouples with the diameter of 0.3mm were embedded in the friction lining which are close to the contact surface. The position of thermocouple is shown in Fig. 6. Firstly, the holes with the diameter of 1mm were drilled on the lateral side of friction lining. Then the oddment of the friction lining was filled in the hole after the thermocouple was embedded. In Fig. 8, points a, b and c were in the central line of rope groove, points d and h were in the middle of contact zone I, points e and f were in the middle of contact zone II and point g was in the middle of contact zone III. The distance from points c, d, f, g and h to the contact surface is about 2mm, and the distance between points e and f, a and b, b and c is about 2mm, too.

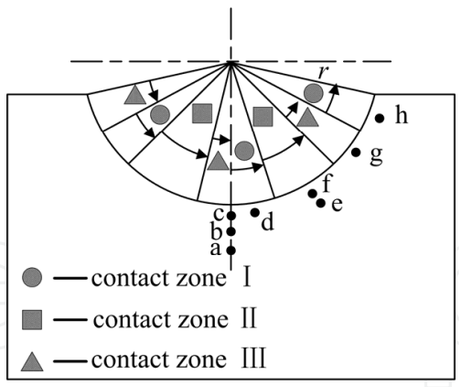

Fig. 6. Layout of thermocouple

2.5.2 Experimental parameters

The sliding speed and the equivalent pressure are the main factors affecting the temperature rise of friction lining during the sliding process. Therefore, the experiments were carried out with different sliding speeds and equivalent pressures. The sliding distance is about 20m. According to the friction experiment standard for friction lining (MT/T 248-91, 1991), the equivalent pressure is 1.5~3MPa. The parameters for the experiment are listed in Table 1.

	v≤10mm/s	v>10mm/s
Equivalent pressure (MPa)	1.5, 2, 2.5, 3	1.5, 2.5
Speed (mm/s)	1, 3, 5, 7, 10	30, 100, 300, 500, 700, 1000

Table 1. Parameters for friction experiment

2.5.3 Experimental results

Fig. 7 shows the partial experiment results within the speed range of 1~10mm/s.

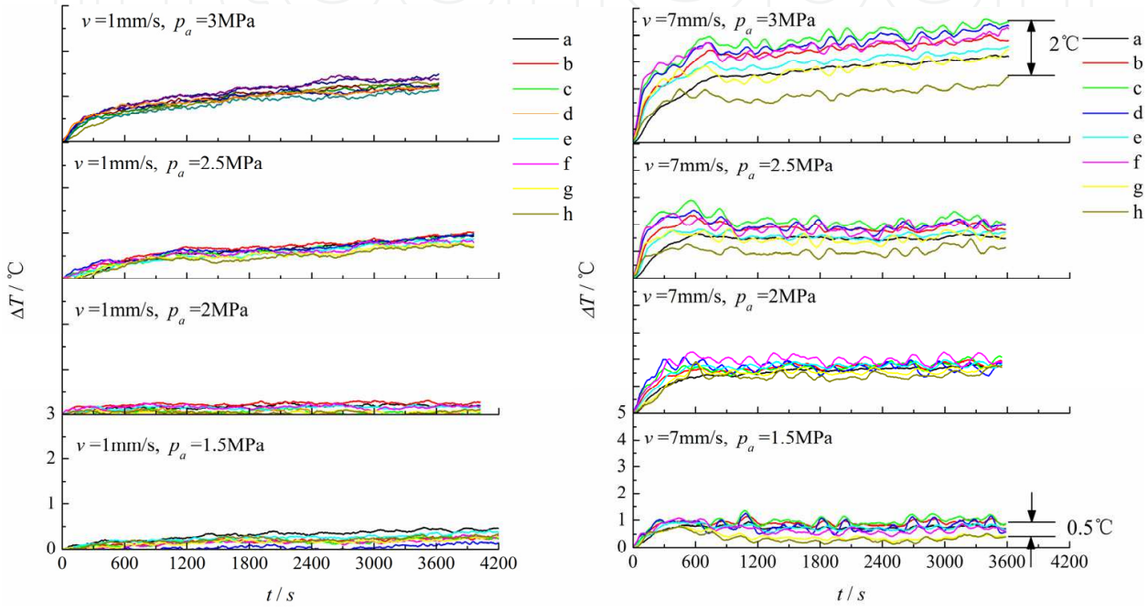

(a) 1mm/s (b) 7mm/s

Fig. 7. Variation of testing points' temperature

As shown in Fig. 7, the temperature rise is less than 5°C within 1 hour when the sliding speed is less than 10mm/s. Therefore, the temperature rise of friction lining can be neglected under the normal hoist condition. It is observed that the temperature increases wavily and the amplitude of waveform increases with the sliding speed. This is due to the periodical heat-flow resulting from the helical contact characteristics. In addition, the temperature difference among 8 points is small and it increases with the equivalent pressure: the temperature difference increases from 0.5°C to 2°C when the equivalent pressure increases to 3MPa. It is found that the temperature increases quickly at the beginning of the sliding process, and then it increases slowly.

In order to analyze the effect of the sliding speed and the equivalent pressure on the temperature, Fig. 8 shows the temperature rise of point c at different sliding speeds and equivalent pressures.

It is seen from Fig. 8 that the sliding speed has stronger effect than the equivalent pressure on the temperature. It is concluded that the sliding speed is more sensitive to the temperature. Therefore, only two equivalent pressures (1.5MPa and 2.5MPa) are selected at the high-speed experiment.

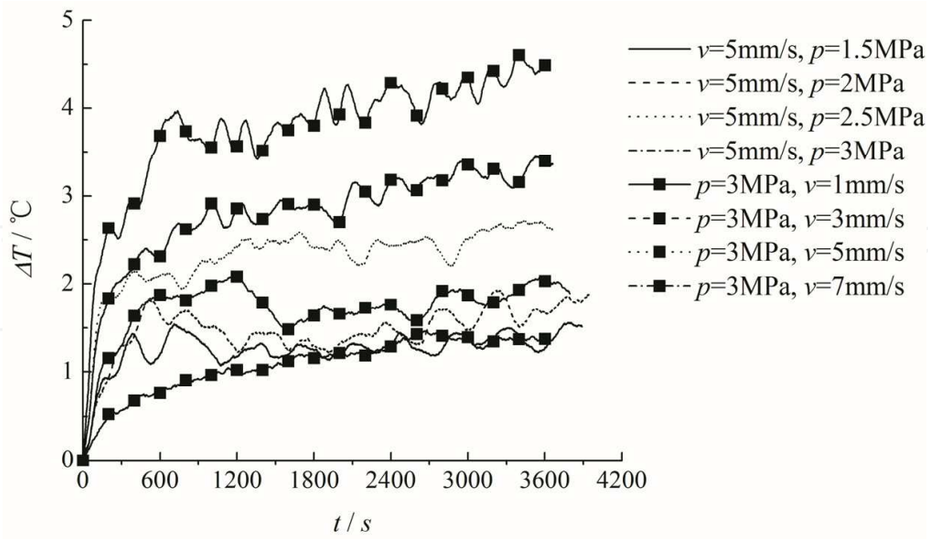

Fig. 8. Effect of speed and equivalent pressure on temperature within low speed

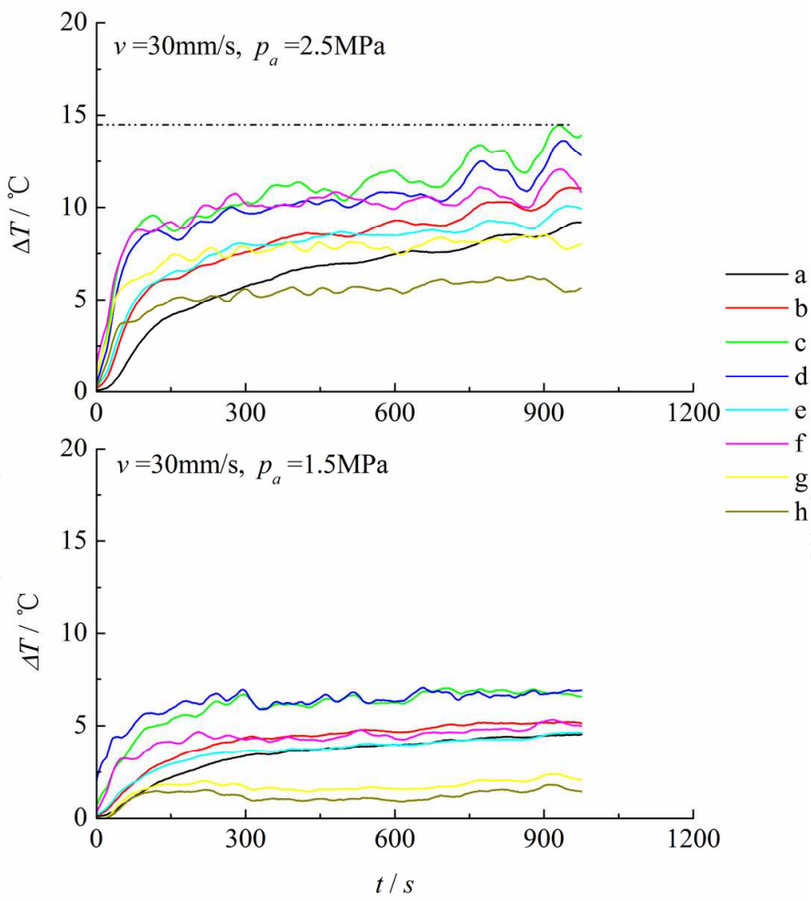

Fig. 9. Variation of testing points' temperature

As show in Fig. 9, the highest temperature rise increases to 15°C at the speed of 30mm/s. Additionally, it is observed that the temperature at points c, d and f is higher than that at other points. However, the temperature rise is not high enough to tell the highest among them.

	Distance between points and point to friction surface / mm (fs-friction surface)							
	a-b	b-c	c-fs	d-fs	e-f	f-fs	g-fs	h-fs
1.5Mpa	2	2	1.8	1.38	2	2.16	2.24	2.24
2.5MPa	1.98	2.06	1.7	2	1.9	1.7	1.48	1.48

Table 2. Position of testing points in friction lining

In order to master the surface temperature of friction lining, the friction experiment was performed with the increasing speed. Table 2 shows the distance of 8 points, and Fig. 10 shows the partial experiment results within the speed range 100~1000mm/s.
It is seen from Fig. 10 that the temperature rise of every point increases obviously. And the order of temperature rise at testing points is shown in Table 3.

Pressure / speed	Order of temperature rise Lining G（high→low）
1.5MPa / 100mm/s	d, c, f, b, e, a, g, h
1.5MPa / 400mm/s	d, c, f, b, e, h, g, a
1.5MPa / 600mm/s	d, f, c, g, h, e, b, a
1.5MPa / 800mm/s	d, c, f, g, e, h, b, a
1.5MPa / 1000mm/s	d, f, c, g, h, e, b, a
2.5MPa / 200mm/s	f, g, c, d, e, h, b, a
2.5MPa / 300mm/s	f, c, g, d, e, h, b, a
2.5MPa / 550mm/s	f, c, g, d, e, h, b, a
2.5MPa / 750mm/s	f, g, c, d, h, e, b, a
2.5MPa / 980mm/s	f, c, d, g, h, e, b, a

Table 3. Order of temperature rise at testing points

The highest temperature rise occurs at point d with p_a=1.5MPa while the highest temperature rise appears at point f with p_a=2.5MPa. This is because that point d is close to the friction surface with the minimize distance of 1.38mm while the distance from point f to friction surface is 2.16mm, which reveals the temperature gradient in the surface layer is high. Therefore, the temperature at point d is higher than that at point f. It is found from Table 3 that the temperature at points f, d and c is higher than that at other points, which is in accordance with the analytical results of the helical contact characteristics and partial heat-flow density. As shown in Fig. 3(b), the contact zone II is subject to the long-time heat-flow and the convection heat transfer of contact zone I at the bottom of the rope groove is worse than that of other zone. Consequently, the temperature at points c, d and f is higher.

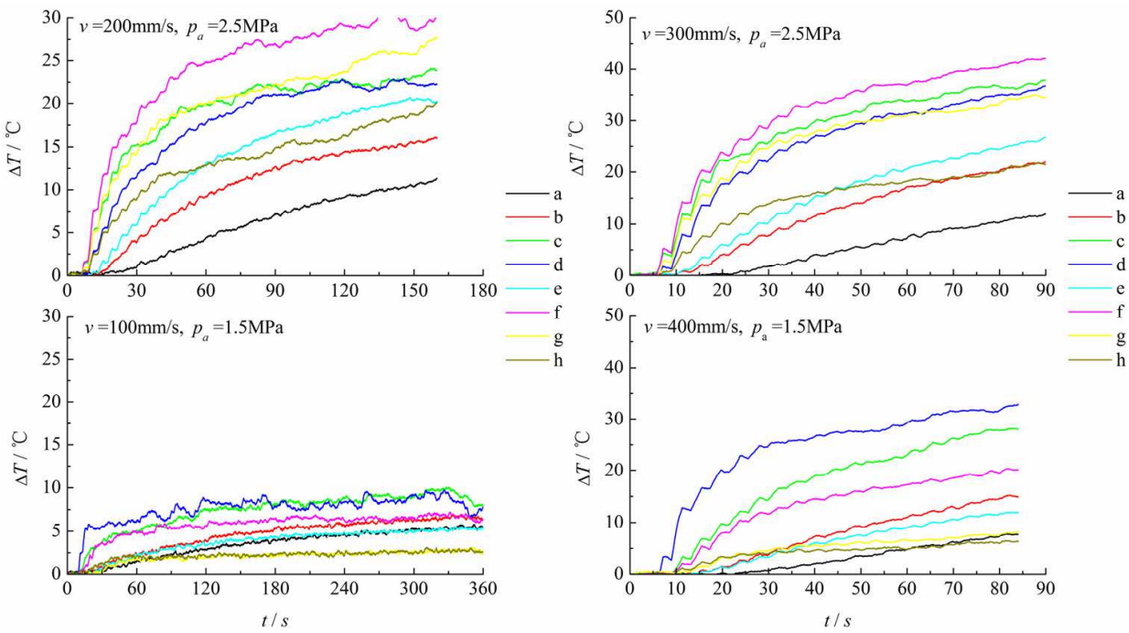

(a) 100-210mm/s

(b) 300-400mm/s

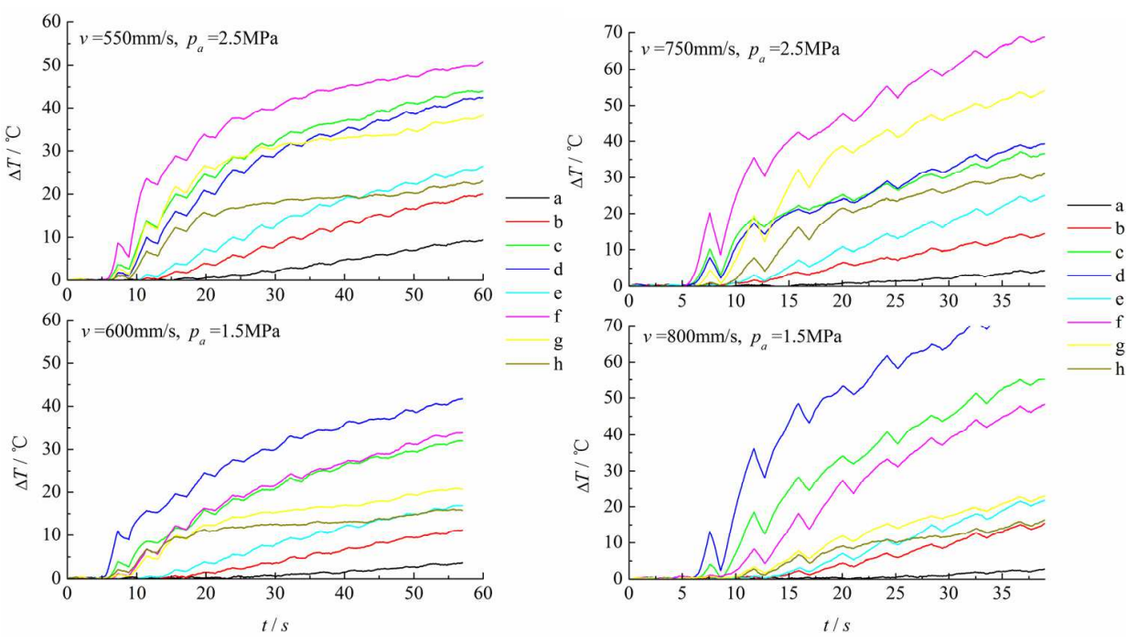

(c) 550-600mm/s

(d) 750-800mm/s

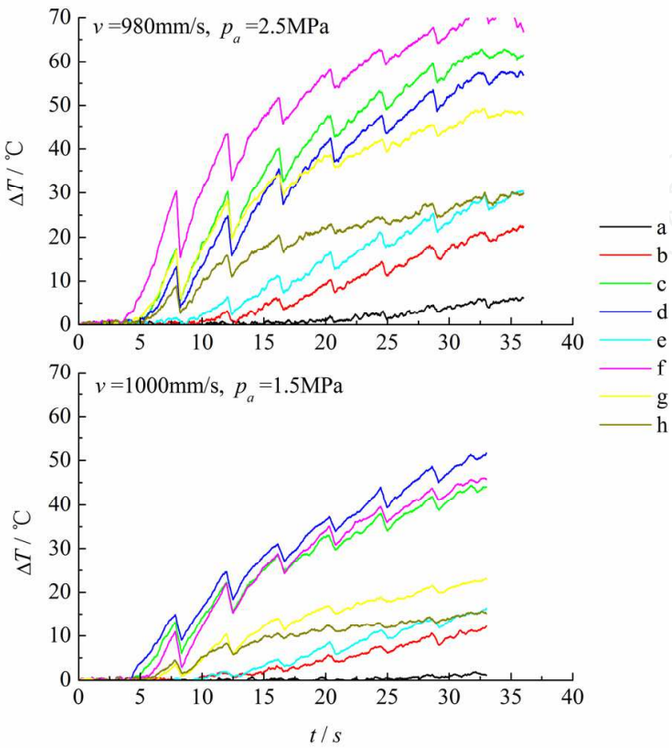

(e) 980-1000mm/s

Fig. 10. Variation of testing points' temperature

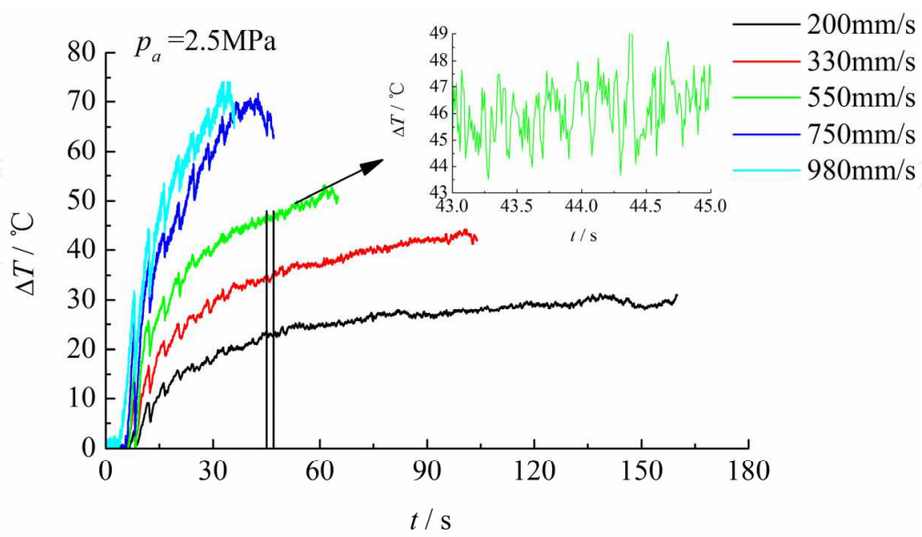

Fig. 11. Variation of temperature rise at point f with speed

The variation of the temperature at point f with the speed is shown in Fig. 11. It is found that the temperature at point f increases with the sliding speed. And the gradient of the temperature rise increases rapidly with the speed at the beginning of the sliding process. Additionally, from the drawing of partial enlargement 550mm/s, the temperature increases periodically which agrees with the helical contact characteristics.

Combining Fig. 10 and Fig. 11, it is found that the temperature rise increases wavily at the initial sliding stage, and the amplitude of wave increases with the sliding speed while it decreases with the time. The explanation for the reduced temperature in the wavy temperature is given as: (a) the rapid temperature rise results in decrease of the mechanical property, and the contact area is enlarged which accelerates the heat exchange between friction lining and wire rope, thus the temperature of friction lining reduces; (b) the increase of contact area reduces the equivalent pressure and the heat-flow decreases rapidly; (c) due to unstable and discontinuous speed at the initial sliding stage, the heat exchange between friction lining and wire rope increases and the temperature decreases in a short time. As the sliding distance increases, the heat exchange tends to balance which decrease the amplitude of the wave.

2.6 Analysis on numerical simulation and experimental results

In order to validate the theoretical model, the theoretical results are compared with the experiment results. The parameters for the experiment are: v=0.55m/s, p_a=2.5MPa. h_1=h_2=h_4=10W/m²K. Supposed that the contact surface of rope groove is only subjected to heat-flow, then h_3=0. r_1=0.014m, r_2=0.04m and T_0=30°C. And the thermophysical properties of wire rope are shown in Table 4.

	ρ_w/ (kg·m^{-3})	C_{pw}/ (J·kg^{-1}·K^{-1})	λ_w / (W·m^{-1}·K^{-1})
Wire rope	7866	473	53.2

Table 4. Thermophysical properties of wire rope

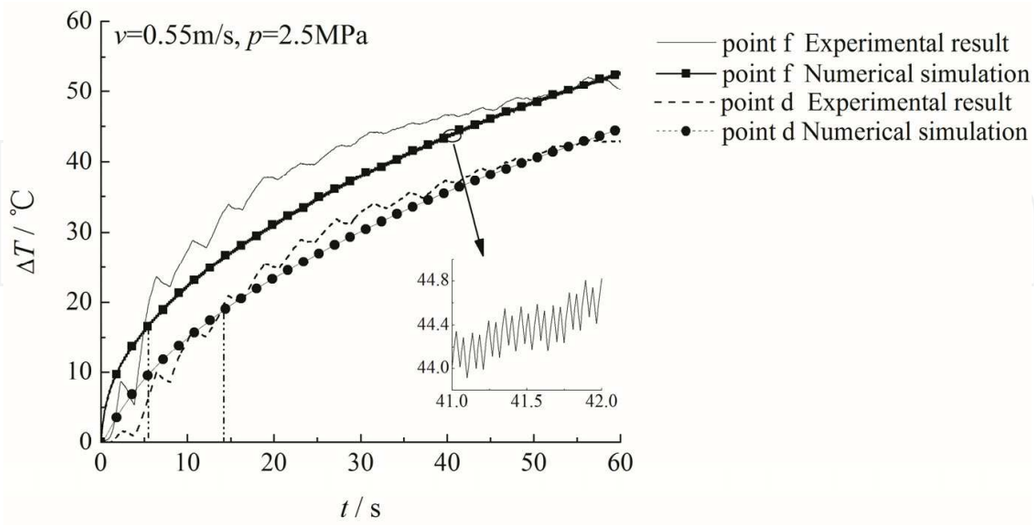

Fig. 12. Comparison between simulation and experimental results

As shown in Fig. 12, the temperature rise at point f increases to 52°C at 60s. From the drawing of the partial enlargement at point f, the simulation result shows that the

temperature increases during the cycle of heat absorption and heat dissipation, which agrees with the experiment results in Fig. 11. At the beginning of the sliding process, the temperature of simulation result is higher than that of experiment results. And the experimental value fluctuates obviously. This is because that the thermocouple absorbs the heat, and the speed at the initial state of sliding process is unstable which leads to the heat conduction for longer time at the local zone. Thus the experimental data is low and the curve of temperature behaves serrasoidal. As the sliding process continues, the experimental value is higher than the simulation value and the both values tend to be equal in the end. This is because that the friction lining is subjected to temperature and stress and the temperature rise results in the increase of surface deformation in the rope groove, which makes the embedding thermocouple closer to the friction surface and leads to the rapid temperature rise of the measuring point. Therefore, the experimental value is higher than the theoretical value: the higher temperature rise at point f makes the deformation bigger and the thermocouple is closer to the surface, which makes the temperature difference between the experimental value and theoretical value at point f is higher than that at point d. When the heat conduction tends to achieve the balance, the temperature variation gets gently and the experimental value is consistent with the theoretical value. Compared the experimental value with the theoretical value in Fig. 12, both of them agree well with each other which validates the theoretical model of the temperature field.

The above analysis indicates that the theoretical model of temperature field is reasonable and correct. Due to difficultly obtaining the temperature of the friction surface by the way of the direct contact measurement, the temperature of the contact surface is simulated in Fig. 13.

As in Fig. 13, the temperature on the friction surface is much higher: though the distance between point f and friction surface is only 2mm, the temperature at friction surface is 18°C higher than that at point f. In addition, the radial temperature gradient at different time is simulated in Fig. 14. The temperature gradient at the surface layer is high and its maximum is about 35000°C/m. And the temperature gradient decreases with the radius. As the sliding process continues, the curve of temperature gradient at the surface layer tends to be flat. The

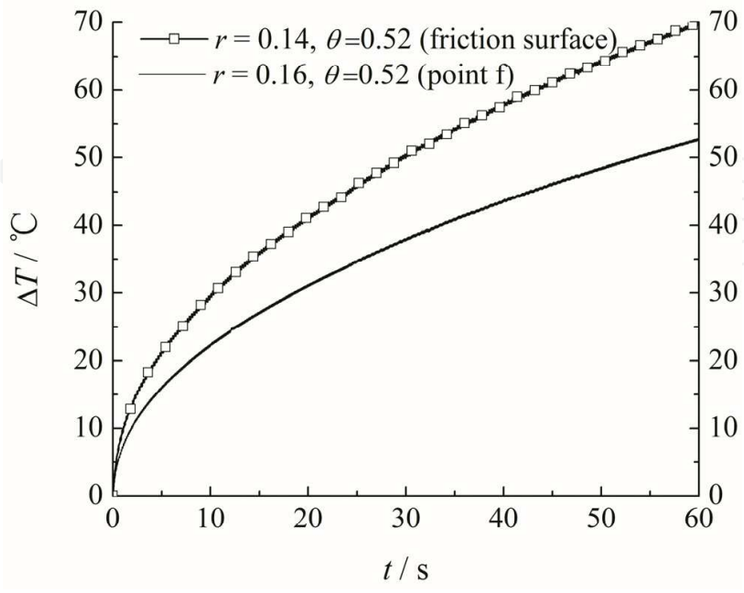

Fig. 13. Variation of temperature on friction surface

above analysis indicates that the heat-conducting property of friction lining is poor. Thus, in order to develop the new friction lining with good thermophysical properties, it is necessary to optimize the ratio of basic material and filler and select the component with good heat-conducting property.

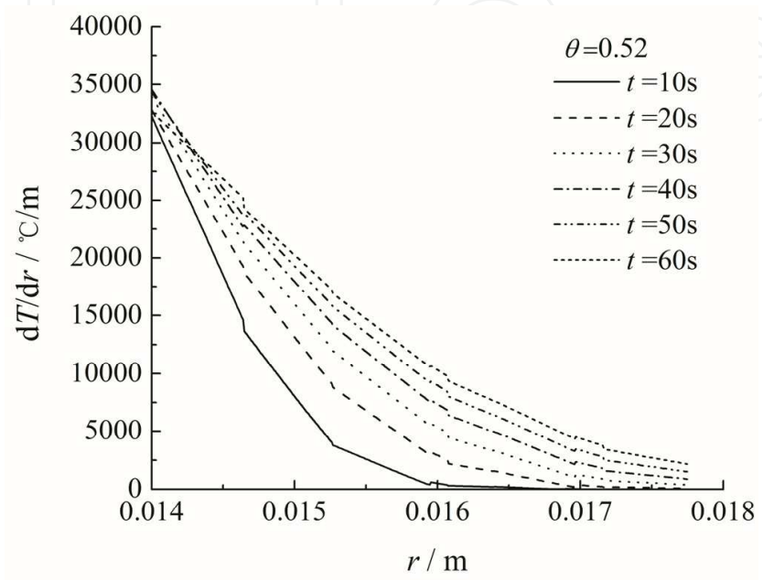

Fig. 14. Radial temperature gradient at different time

3. Heat conduction for periodical contact

3.1 Theoretical model

As shown in Fig. 1, the disc brake for mine hoist is composed of brake disc and brake shoes. During the braking process, the brake shoes are pushed onto the disc with a certain pressure, and the friction force generated between them is applied to brake the drum of mine hoist.

The heat energy caused by the friction between brake shoes and brake disc leads to their temperature rise. However, the two important parts have different behaviors of heat conduction: the brake shoe is subjected to continuous heat while the brake disc is heated periodically due to rotational motion. And the two types of temperature field will be discussed as follows.

3.1.1 Dynamic thermophysical properties of brake shoe

In order to obtain the temperature field of disc brake, it is necessary to obtain their thermophysical properties. As the brake shoe is a kind of composite material, its dynamic thermophysical properties (DTP) (specific heat capacity c_s, thermal diffusivity a_s and thermal conductivity l_s) vary with the temperature. And the testing results (Bao, 2009) are shown in Fig. 15.

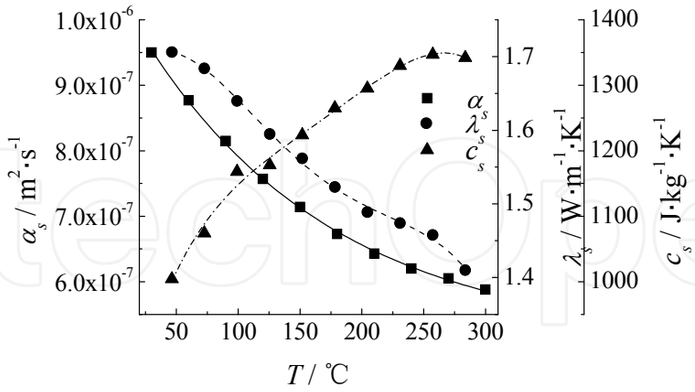

Fig. 15. Dynamic thermophysical properties of brake shoe

According to the data in Fig. 15, the fitting equations of DTP are gained by regression analysis

$$\begin{aligned}
&\alpha_s = 0.509 + e^{-\frac{T-30}{153.843}},\\
&\lambda_s = 1.694 + 1.21\times10^{-3}T - 3\times10^{-5}T^2 + 1.436\times10^{-7}T^3 - 2.144\times10^{-10}T^4,\\
&c_s = 0.864 + 5.59\times10^{-3}T - 4\times10^{-5}T^2 + 1.56\times10^{-7}T^3 - 2.3\times10^{-10}T^4.
\end{aligned} \tag{16}$$

The brake disc is a kind of steel material, and it is generally assumed that its thermophysical properties are invariable during the braking process. And its static thermophysical parameters (STP) are shown in Table 5.

ρ_d [kg·m^{-3}]	c_d [J·kg^{-1}·K^{-1}]	λ_d [W·m^{-1}·K^{-1}]
7866	473	53.2

Table 5. Static thermophysical parameters of brake disc

Accordingly, the dynamic distribution coefficient of heat-flux is obtained (Zhu, 2009):

$$\begin{aligned}
k_s &= \frac{1}{1+\sqrt{\frac{\rho_d c_d \lambda_d}{\rho_s c_s \lambda_s}}},\\
k_d &= 1 - k_s,
\end{aligned} \tag{17}$$

where k_s and k_d are the dynamic distribution coefficient of heat-flux for brake shoe and brake disc, respectively.

Combining Eq. (16) and Eq. (17), the dynamic distribution coefficient of heat-flux is plotted in Fig. 16. The curves show that the distribution coefficient of heat-flux for the brake disc always exceeds 0.88, and it absorbs most of heat energy. And k_d decreases with the temperature until 270°C, then it increases above 270°C. According to Eq. (17), k_s has the reverse variation.

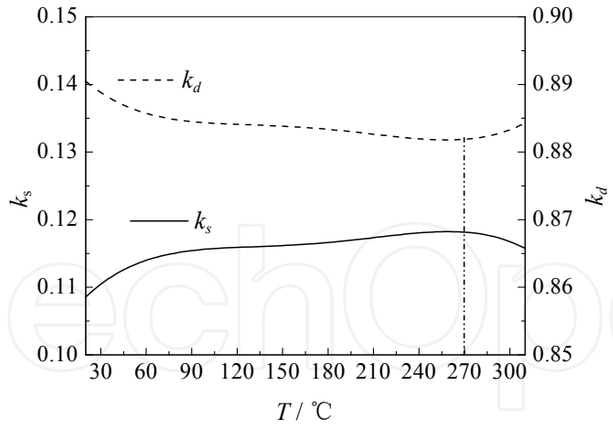

Fig. 16. Dynamic distribution coefficient of heat-flux

3.1.2 Partial differential equation of heat conduction

As shown in Fig. 17, the cylindrical coordinate is used to describe their geometry. Based on the theory of heat conduction, the transient models of disc brake's temperature field are as follows:

$$\rho_s c_s \frac{\partial T_s}{\partial t} = \frac{1}{r_s}\frac{\partial}{\partial t}\left(\lambda_s r_s \frac{\partial T_s}{\partial r_s}\right) + \frac{1}{r_s^2}\frac{\partial}{\partial \theta_s}\left(\lambda_s \frac{\partial T_s}{\partial \theta_s}\right) + \frac{\partial}{\partial z_s}\left(\lambda_s \frac{\partial T_s}{\partial z_s}\right), \tag{18}$$

$$\frac{\rho_d c_d}{\lambda_d}\frac{\partial T_d}{\partial t} = \frac{1}{r_d}\frac{\partial}{\partial t}\left(r\frac{\partial T_d}{\partial r_d}\right) + \frac{1}{r_d^2}\frac{\partial^2 T_d}{\partial \theta_d^2} + \frac{\partial^2 T_d}{\partial z_d^2}. \tag{19}$$

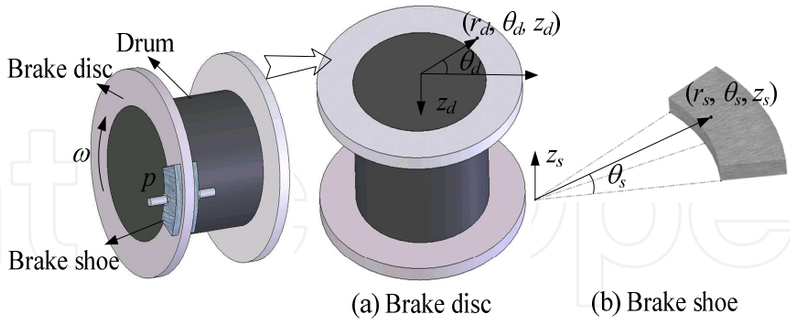

Fig. 17. Geometry Model of disc brake

3.1.3 Heat-flux

Suppose that the friction heat energy is absorbed completely by the brake shoe and brake disc

$$\begin{aligned} q &= q_d + q_s, \\ q_d &= k_d q,\ q_s = k_s q, \end{aligned} \tag{20}$$

where q is the whole heat-flux, q_d and q_s are the disc's and shoe's heat-flux, respectively. And the

$$q(r,t) = f \cdot p(t) \cdot v(t) = f \cdot p(t) \cdot \omega(t) \cdot r, \tag{21}$$

where f is the coefficient of friction between brake disc and brake shoe, p is the brake pressure, v and w are the linear and angular velocity. The brake pressure pushed onto the brake disc increases gradually, and the pressure is given as (Cao & Lin, 2002)

$$p(t) = p_0\left(1 - e^{-\frac{t}{t_z}}\right), \tag{22}$$

where p_0 is the initial brake pressure, and t_z is total braking time. In addition, the angular velocity is assumed to decrease linearly, then

$$\omega = \omega_0\left(1 - \frac{t}{t_z}\right), \tag{23}$$

where $\omega_0 = v_0/r_0$, v_0 is the initial linear velocity and r_0 is the average radius.

Combining Eq.(21), Eq.(22) and Eq.(23), the whole heat-flux is gained as following

$$q(r,t) = f \cdot p_0 \cdot \omega_0\left(1 - e^{-\frac{t}{t_z}}\right) \cdot \left(1 - \frac{t}{t_z}\right) \cdot r. \tag{24}$$

3.1.4 Boundary conditions

During the barking process, the brake disc rotates while the brake shoe keeps static. Therefore, the brake disc and brake shoe have different boundary conditions. For the brake shoe, its friction surface is subjected to the constant heat-flux.

$$q_{sf} = q_s, r_s \in (r_1, r_2), t \in (0, t_z), z_s = 0. \tag{25}$$

With regard to the fixed area in the brake disc, it is subject to the periodical heat-flux. In order to calculate the temperature rise of brake disc, the movable heat-flux is expressed by

$$\begin{aligned} &q_{df} = q_d, \quad \theta_d \in (\theta_1 - \theta_0, \theta_1 + \theta_0), r_d \in (r_1, r_2), z_d = 0 \\ &\theta_1 = \int_0^t \omega(t)\mathrm{d}t = \omega_0\left(t - \frac{t^2}{2t_z}\right). \end{aligned} \tag{26}$$

where $\theta_1 = \theta_1 - 2n\pi, n = \theta_1 \bmod 2\pi$.

3.2 Results and discussion

According to the above theory analysis, the temperature rise of brake shoe and brake disc is simulated by finite element method. The dimension parameters are as follows: $r_1 = 2.35$,

$r_2 = 2.55$, $r_0 = (r_1 + r_2)/2$, $\theta_d \in (0, 2\pi)$, $\theta_0 = -0.0612$, $r_d \in (-0.03, 0)$, $r_s \in (0, 0.025)$. The braking parameters are shown in Table 6. And Figs. 18-23 show the simulation results.

f	p [MPa]	v_0 [m·s^{-1}]	t_z [s]
0.4	1.36	10	7.32

Table 6. Braking parameters for disc brake

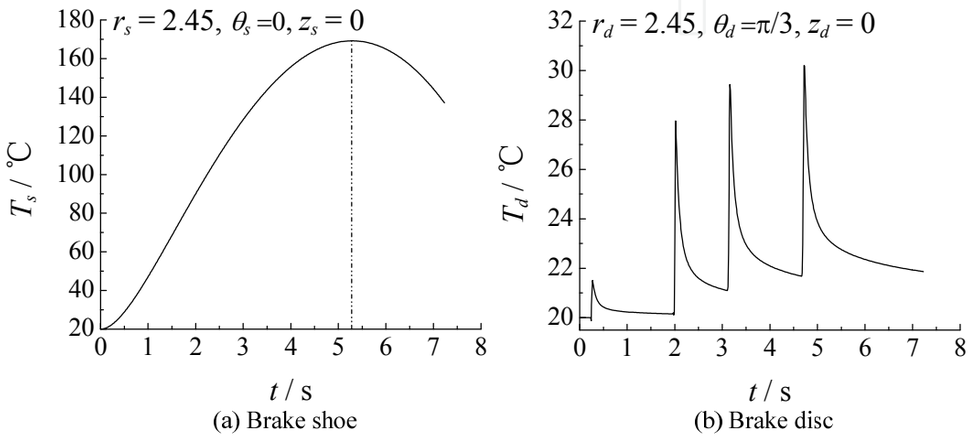

Fig. 18. Temperature rise of disc brake

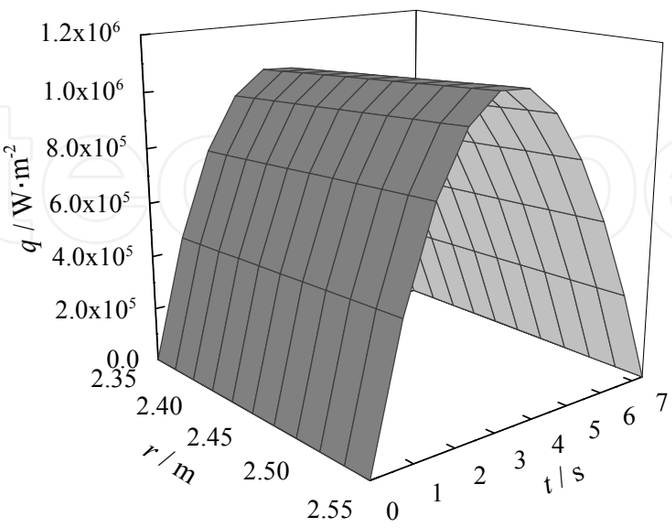

Fig. 19. Variation of heat-flux with t and r

It is seen from Fig. 18 that DTP has little effect on the temperature rise. The brake shoe's temperature calculated with DTP is a little higher than that with STP, while the temperature of brake disc with DTP is in accordance with that with STP. In Fig. 18, the temperature of brake shoe varies smoothly while the temperature of brake disc changes periodically. In Fig. 18(a), the temperature of brake shoe increases with the time and reaches the maximum 169°C at t = 5.3s, then it decreases. This result agrees with the variation of heat-flux in Fig. 19: there is a peak in the curve of heat-flux during the braking process. Though the brake disc absorbs most of friction heat, its maximal temperature, which is only 30°C, is much lower than brake shoe's. With regard to the fixed point in brake disc, it is subject to heat-flux within short time and convects with the air in most time of every circle. Thus, the temperature of brake disc is lower and varies periodically.

In addition, the temperature of fixed point at different q_{d} in a circle is simulated, and the simulation results are in Fig. 20. The peak of temperature occurs when the point on the disc contacts with the shoe. And the variation of temperature peak agrees well with the variation of heat-flux during the braking process. Furthermore, the variation of temperature with radius is shown in Fig. 21. The temperature of brake shoe increases with the radius slightly for minor difference between inner and outer radius. The temperature on both edges of the contact zone in brake disc is low, while it is high in the middle.

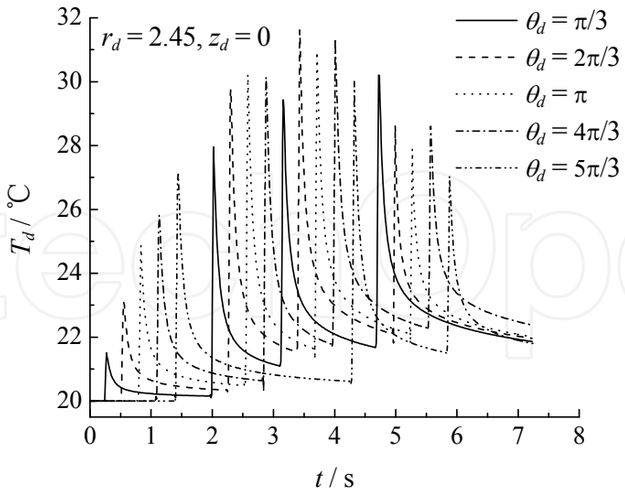

Fig. 20. Variation of T_{d} with q_{d}

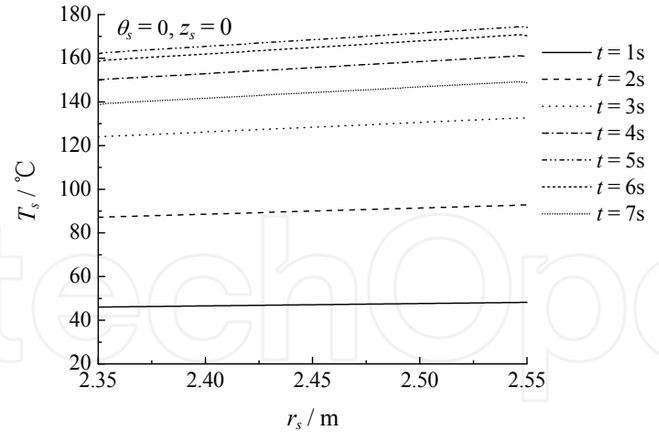

(a) brake shoe

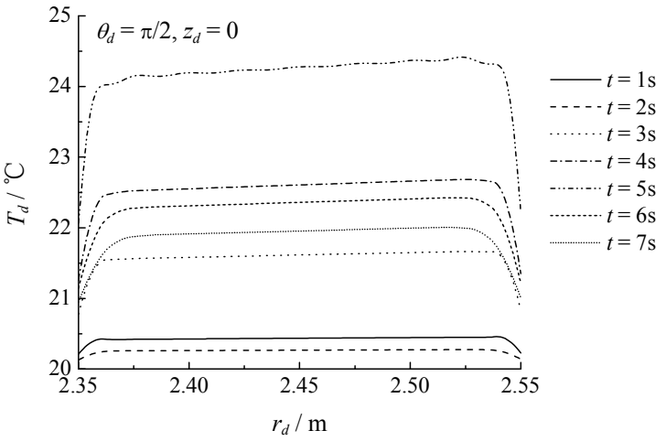

(b) brake disc

Fig. 21. Variation of temperature with radius

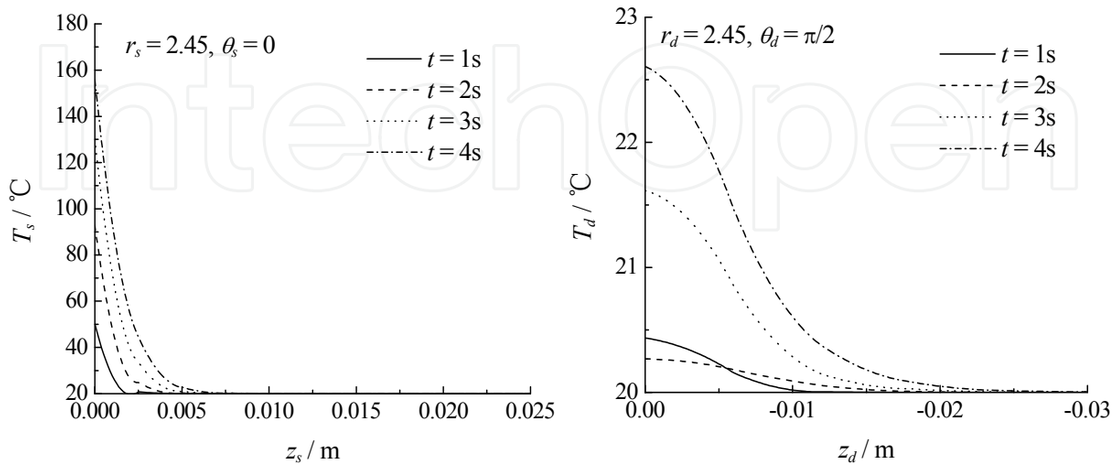

(a) brake shoe (b) brake disc

Fig. 22. Variation of temperature with depth

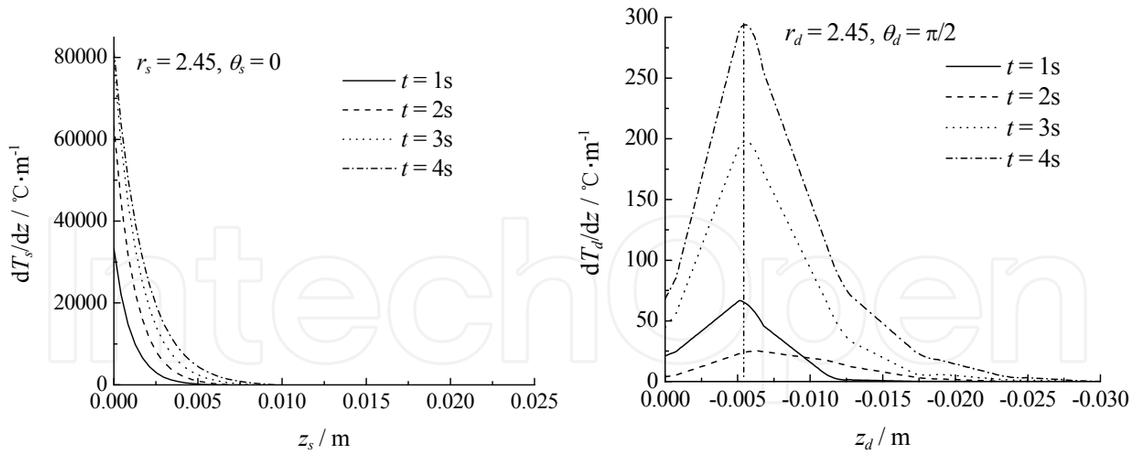

(a) brake shoe (b) brake disc

Fig. 23. Variation of temperature gradient with depth

From Figs. 22 and 23, the temperature of brake shoe decreases sharply with z_d: it reduced to zero at z_s=0.0075m. And the temperature gradient on the friction surface is the highest: the maximum of temperature gradient is up to 8×10^4℃·m^{-1} at t = 4s. These results show that the friction heat energy concentrates on the surface layer and the brake shoe's heatconducting property is poor. However, the temperature rise of brake disc decreases to zero after z_d = -0.025m and its maximum is only 300℃·m^{-1} at t = 4s. Additionally, it is found that the maximum of brake disc's temperature gradient is not on the friction surface and it appears at z_d = -0.006m. Due to the high thermal conductivity of the brake disc and surface heat convection, the speed of heat dissipation is fast on the surface. But the inner surface has the low speed of heat transfer. Therefore, though its surface temperature is the highest, but the maximum of temperature gradient occurs at z_d = -0.006m of the inner surface. These results reveal that the brake disc's heatconducting property is better than brake shoe's.

4. Conclusions

1. The friction lining contacts with the outside of rope strand periodically and the number of contact point is two or three. Additionally, the rope groove of friction lining is divided into three contact zones and the contact arcs are unequal: the contact arc in the contact zone II is the longest, and the contact arcs in the contact zones I and III are equal.
2. The thermophysical properties of lining K is lower than that of ling G. As the testing temperature increases, the specific heat capacity increases with the temperature, the thermal diffusivity decreases with the temperature nonlinearly and the thermal conductivity□increases with the temperature below 90°C and keeps approxistable above 90°C.
3. According to the force analysis of friction lining under the operating condition and experimental condition, the total heat-flow under the two situations is obtained. And

the partial heat-flow corresponding to every contact zone is obtained based on the helical contact characteristic.

4. With the consideration of the thermophysical properties and helical non-complete contact characteristics, the theoretical model of friction lining's transient temperature field is established, and the finite difference method is adopted to solve this problem.
5. The friction experiment indicates that the temperature of friction lining increases with the equivalent pressure and sliding speed and the sliding speed has stronger effect than the equivalent pressure on the temperature. During the low-speed sliding, the temperature rises gently and the temperature at the measuring points is approximately equal. The temperature rise is less than 5 °C within 1 hour when the sliding speed is less than 10mm/s. And the highest temperature rise increases to 15°C at 30mm/s. As the speed increases to 1000mm/s, the temperature rise at every point increases obviously. Additionally, the temperature rise increases wavily at the initial sliding stage and the amplitude of the wave increases with the sliding speed while it decreases with the time. Furthermore, the temperature increases periodically which agrees with the helical contact characteristics.
6. The simulation result agrees with the experiment result, which validate the theoretical model of the temperature field. The temperature on the contact surface and the temperature gradient were simulated under the experimental condition (v=0.55m/s, p_a=2.5MPa). The simulation result indicates that the friction heat focuses on the contact surface layer and the temperature gradient on the surface layer is the highest. In addition, the heat-conducting property of friction lining is poor. In order to develop the new friction lining with good thermophysical properties, it is necessary to optimize the ratio of basic material and filler and selected the component with good heat-conducting property.
7. Combining dynamic thermophysical properties of brake shoe and dynamic distribution coefficient of heat-flux, the theoretical models of brake shoe and brake disc's temperature field were established. And the static and periodical heat-flux on the friction surface of brake shoe and brake disc were obtained.
8. DTP of brake shoe has little effect on the temperature. The temperature of brake shoe varies smoothly while that of brake disc changes periodically. The maximal temperature of the brake disc is much lower than that of the brake shoe during the braking process. And the variation of temperature rise's peak at different $\square_d$ agrees well with the variation of heat-flux during the braking process. Additionally, the temperature of disc brake increases with the radius slightly.
9. The temperature of brake shoe and brake disc decreases with the depth, and the temperature gradient of brake shoe is much higher than that of brake disc. In addition, the maximum of brake disc's temperature gradient is not on the friction surface and it appears at z_d = -0.006m. The friction heat energy concentrates on the surface layer of brake shoe and the heatconducting property of brake disc is better than that of brake shoe.

5. Acknowledgements

This project is supported by the National Natural Science Foundation of China (Grant No. 51105361), the China Postdoctoral Science Foundation funded project (Grant No. 20100481179), Fundamental Research Funds for the Central Universities (Grant No.

2010QNA25), National High Technology Research and Development Program of China (863 Program) (Grant No. 2009AA04Z415), National Natural Science Foundation of China (Grant No. 50875253) and Natural Science Foundation of Jiangsu Province (Grant No. BK2008127).

6. References

Editorial Committee of Mine Safety Handbooks, Editor, (2004). *Safety Regulations for Coal Mine*, China Coal Industry Publishing House, Beijing.

Peng,Y.X., Zhu, Z.C., Chen, G.A. (2008). Numerical simulation of lining's transient temperature field during friction hoist's sliding. *J. Chin. Univ. Min. Technol.*, Vol. 37, No. 4, (2008), pp. 526-531. (in Chinese)

Liu, D.P., Mei, S.H. (1997). Approximate method of calculating friction temperature in friction winder lining. *J. Chin. Univ. Min. Technol.,* Vol. 26, No. 1, (1997), pp. 70-72. (in Chinese)

Xia, R.H. Ge S.R. (1990). Calculation of temperature rise of lining of friction winder. *J. Chin. Coal Soc.*, Vol. 15, No. 2, (1990), pp. 1-9. (in Chinese)

Yang, Z.J. (1990). Theoretical calculation of the lining's temperature field of multi-rope friction winder. *J. Shanxi Min. Inst.*, Vol. 8, No. 4, (1990), pp. 304-314. (in Chinese)

Singh, K., Singh, A.K. Saxena, N.S. (2008). Temperature dependence of effective thermal conductivity and effective thermal diffusivity of $Se_{90}In_{10}$ bulk chalcogenide glass. *Curr. Appl. Phys.*, Vol. 8, No. 2, (2008), pp. 159-162.

Isoda, H., Kawashima, R. (2007). Temperature dependence of thermal property for lead nitrate crystal. *J. Phys. Chem. Solids.*, Vol. 68, No. 4, (2007), pp. 561-563.

He, W., Liao, G.X., Liu, C. (2005). Thermal and dynamic mechanical properties of PPESK/PTFE blends. *Chin. J. Mater. Res.*, Vol. 19, No. 5, (2005), pp. 464-470. (in Chinese)

Hegeman, J.B.J., van der Laan, J.G., van Kranenburg, M., Jong, M., d'Hulst, D., ten Pierick, P. (2005). Mechanical and thermal properties of SiC_f/SiC composites irradiated with neutrons at high temperatures. *Fusion Eng. Des.*, Vol. 75-79, (2005), pp. 789-793.

Mazzone, A.M. (2005). Thermal properties of clustered systems of mixed composition: the temperature response of Si-Al clusters studied quantum mechanically. *Comput. Mater. Sci.*, Vol. 34, No. 1, (2005), pp. 64-69.

Golebiowski, J., Kwieckowski, S. (2002). Dynamics of three-dimensional temperature field in electrical system of floor heating. *Int. J. Heat Mass Transfer*, Vol. 45, No. 12, (2002), pp. 2611-2622.

Lukyanov, S. (2001). Finite temperature expectation values of local fields in the sinh-Gordon model. *Nucl. Phys. B.*, Vol. 612, No. 3, (2001), pp. 391-412.

Matysiak, S.J., Yevtushenko, A.A., Ivanyk, E.G. (2002). Contact temperature and wear of composite friction elements during braking. *Int. J. Heat Mass Transfer*, Vol. 45, No. 1, (2002), pp. 193-199.

Yevtushenko, A.A., Ivanyk, E.G. (1997). Determination of temperatures for sliding contact with applications for braking systems. *Wear*. Vol. 206, No. 1-2, (1997), pp. 53-59.

Naji, M., Al-Nimr, M. (2001). Dynamic thermal behavior of a brake system. *Int. Commun. Heat Mass Transfer.*, Vol. 28, No. 6, (2001), pp. 835-845.

Zhu, Z.C., Peng, Y.X., Shi, Z.Y., Chen, G.A. (2009). Three-dimensional transient temperature field of brake shoe during hoist's emergency braking. *Appl. Therm. Eng.*, Vol. 29, No. 5-6, (2009), pp. 932-937.

Voldrich, J. (2007). Frictionally excited thermoelastic instability in disc brakes-transient problem in the full contact regime. *Int. J. Mech. Sci.*, Vol. 49, No. 2, (2007), pp. 129-137.

Qi, H.S. Day, A.J. (2007). Investigation of disc/pad interface temperatures in friction braking. *Wear*, Vol. 262. No. 5-6, (2007), pp. 505-513.

Thuresson, D. (2006). Stability of sliding contact-comparison of a pin and a finite element model. *Wear*, Vol. 261, No. 7-8, (2006), pp. 896-904.

Choi, J.H., Lee, I. (2004). Finite element analysis of transient thermoelastic behaviors in disk brakes. *Wear*, Vol. 257, No. 1-2, (2004), pp. 47-58.

Chang, L.Z., Li, B.Z. (2008). Numerical simulation of temperature fields in electroslag remelting slab ingots. *Acta Metall. Sinica.*, Vol. 21, No. 4, (2008), pp. 253-259.

Liu, X., Yao, J., Wang, X., Zou, Z., Qu, S. (2009). Finite difference modeling on the temperature field of consumable-rod in friction surfacing. *J. Mater. Process. Technol.*, Vol. 209, No. 3, (2009), pp. 1392-1399.

Zhu, Z.C., Shi, Z.Y., Chen, G.A. (2008). Experimental Study on Friction Behaviors of Brake Shoes Materials for Hoist Winder Disc Brakes. *J. Harbin Inst. Techol.*, Vol. 40, No. 3, (2008), pp. 462-465. (In Chinese)

Zhu, Z.C., Shi, Z.Y., Chen, G.A. (2006). Tribological Behaviors of Asbestos-free Brake Shoes for Hoist Winder Disc Brakes. *Lubr. Eng.*, No. 12, (2006), pp. 99-101. (In Chinese)

Cao, C.H., Lin, X.Z. (2002). Transient Temperature Field Analysis of a Brake in a Non-axisymmetric Three-dimensional Model. *J. Mater. P. T.*, Vol. 129, No. 1-3, (2002), pp. 513-517.

Wang, Y., Cao, X.K., Yao, A.Y., Li, L.Z. (2001). Study on the Temperature Field of Disc Brake Friction Flake. *J. Wuhan U. T.*, Vol. 23, No. 7, (2001), pp. 22-24. (In Chinese)

Lin, X.Z., Gao, C.H., Huang, J.M. (2006). Effects of Operating Condition Parameters on Distribution of Friction Temperature Field on Brake Disc. *J. Eng. Des.*, Vol. 13, No. 1, (2006), pp. 45-48. (In Chinese)

Ma, B.J., Zhu, J. (1999). Contact Surface Temperature Model for Disc Brake in Braking. *J. Xian Inst. Tech.*, Vol. 19, No. 1, (1999), pp. 35-39. (In Chinese)

Ma, B.J., Zhu, J. (1998). The Dynamic Heat Flux Model for Emergency Braking. *Mech. Sci. Tech.*, Vol. 17, No. 5, (1998), pp. 698-700. (In Chinese)

Bao, J.S., Zhu, Z.C., Yin, Y., Peng, Y.X. (2009). A Simple Method for Calculating Maximal Surface Temperature of Mine Hoister's Brake Shoe During Emergency Braking. *J. Comput. Theor. Nanosci.*, Vol. 6, No. 7, (2009), pp. 1566-1570.

MT/T 248-91, (1991). *Testing method for coefficient of friction of lining in friction hoist* [China Coal Industry Standards] (in Chinese)

Bao, J.S. (2009). *Tribological Performance and Its Catastrophe Behaviors of Mine Hoister's Brake Shoe During Emergency Braking*. [Ph.D. Dissertation], China University of Mining and Technology, Xuzhou (2009). (in Chinese)

Heat Transfer - Engineering Applications
Edited by Prof. Vyacheslav Vikhrenko

ISBN 978-953-307-361-3
Hard cover, 400 pages
Publisher InTech
Published online 22, December, 2011
Published in print edition December, 2011

Heat transfer is involved in numerous industrial technologies. This interdisciplinary book comprises 16 chapters dealing with combined action of heat transfer and concomitant processes. Five chapters of its first section discuss heat effects due to laser, ion and plasma-solid interaction. In eight chapters of the second section engineering applications of heat conduction equations to the curing reaction kinetics in manufacturing process, their combination with mass transport or ohmic and dielectric losses, heat conduction in metallic porous media and power cables are considered. Analysis of the safety of mine hoist under influence of heat produced by mechanical friction, heat transfer in boilers and internal combustion engine chambers, management for ultrahigh strength steel manufacturing are described in this section as well. Three chapters of the last third section are devoted to air cooling of electronic devices.

INTECH
open science | open minds

InTech Europe
University Campus STeP Ri
Slavka Krautzeka 83/A
51000 Rijeka, Croatia
Phone: +385 (51) 770 447
Fax: +385 (51) 686 166
www.intechopen.com

InTech China
Unit 405, Office Block, Hotel Equatorial Shanghai
No.65, Yan An Road (West), Shanghai, 200040, China
中国上海市延安西路65号上海国际贵都大饭店办公楼405单元
Phone: +86-21-62489820
Fax: +86-21-62489821

IntechOpen